

Article

Synthesis, Crystal Structural Investigations, and DFT Calculations of Novel Thiosemicarbazones

Brian J. Anderson *, Jerry P. Jasinski, Michael B. Freedman, Sean P. Millikan, Kelly A. O'Rourke and Victoria A. Smolenski

Department of Chemistry, Keene State College, 229 Main Street, Keene, NH 03435-2001, USA; jjasinski@keene.edu (J.P.); mbfreedman92@gmail.com (M.B.F.); seanmilli24@gmail.com (S.P.M.); kellyorourke12@gmail.com (K.A.O.); Victoria.Smolenski@ksc.keene.edu (V.A.S.)

* Correspondence: banderson1@keene.edu; Tel.: +1-603-358-2560

Academic Editor: Helmut Cölfen

Received: 8 January 2016; Accepted: 28 January 2016; Published: 2 February 2016

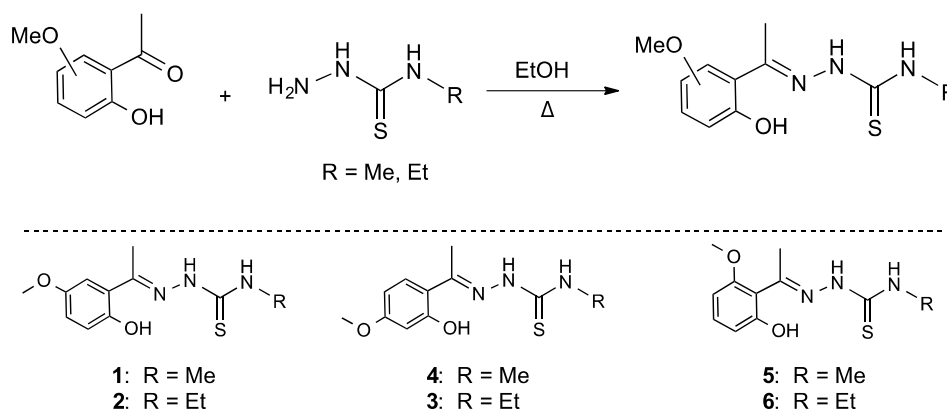
Abstract: The crystal and molecular structures of three new thiosemicarbazones, 2-[1-(2-hydroxy-5-methoxyphenyl)ethylidene]-*N*-methyl-hydrazinecarbothioamide monohydrate (1), 2-[1-(2-hydroxy-5-methoxyphenyl)ethylidene]-*N*-ethyl-hydrazinecarbothioamide (2) and 2-[1-(2-hydroxy-4-methoxyphenyl)ethylidene]-*N*-ethyl-hydrazinecarbothioamide acetonitrile solvate (3), are reported and confirmed by single crystal X-ray diffraction, NMR and UV-vis spectroscopic data. Compound (1), C₁₁H₁₅N₃O₂S·H₂O, crystallizes in the monoclinic with space group P2₁/c, with cell parameters $a = 8.2304(3)$ Å, $b = 16.2787(6)$ Å, $c = 9.9708(4)$ Å, and $\beta = 103.355(4)^\circ$. Compound (2), C₁₂H₁₇N₃O₂S, crystallizes in the C2/c space group with cell parameters $a = 23.3083(6)$ Å, $b = 8.2956(2)$ Å, $c = 13.5312(3)$ Å, $\beta = 91.077(2)^\circ$. Compound (3), C₁₁H₁₅N₃O₂S·C₂H₃N, crystallizes in the triclinic P-1 space group with cell constants $a = 8.9384(7)$ Å, $b = 9.5167(8)$ Å, $c = 10.0574(8)$ Å, $\alpha = 110.773(7)^\circ$, $\beta = 92.413(6)^\circ$, and $\gamma = 90.654(7)^\circ$. DFT B3LYP/6-31(G) geometry optimized molecular orbital calculations were also performed and frontier molecular orbitals of each compound are displayed. The correlations between the calculated molecular orbital energies (eV) for the surfaces of the frontier molecular orbitals to the electronic excitation transitions from the absorption spectra of each compound have been proposed. Additionally, similar correlations observed among three closely related compounds, (4), 2-[1-(2-hydroxy-4-methoxyphenyl)ethylidene]-*N*-methyl-hydrazinecarbothioamide, (5), 2-[1-(2-hydroxy-6-methoxyphenyl)ethylidene]-*N*-methyl-hydrazinecarbothioamide acetonitrile monosolvate and (6), 2-[1-(2-hydroxy-6-methoxyphenyl)ethylidene]-*N*-ethyl-hydrazinecarbothioamide, examining structural differences from the substitution of the methoxy group from the phenyl ring (4, 5, or 6 position) and the substitution of the terminal amine (methyl or ethyl) to their frontier molecular orbital surfaces and from their Density Functional Theory (DFT) molecular orbital energies provide further support for the suggested assignments of the title compounds.

Keywords: thiosemicarbazones; crystal structure; hydrogen bonds; B3LYP 6-31(G); DFT molecular orbital calculations; frontier molecular orbitals

1. Introduction

Thiosemicarbazones are a versatile class of ligands that bind a metal through a nitrogen and sulfur atom. This class of ligands has been widely studied due to their interesting coordination chemistry, prompting several reviews [1–4]. Metal complexes with thiosemicarbazone ligands have been found to have biological activity including anti-malarial [5] and anti-cancer properties [6]. Studies have also looked at the ability of these complexes to bind DNA [7] and they have even been investigated as biological imaging agents [8]. Additionally, recent research has shown metal thiosemicarbazone complexes to be effective catalysts for Heck couplings [9], hydrogenations [10], and

Hartwig couplings [11]. Due to these areas, there is an interest in developing novel thiosemicarbazone compounds and their metal complexes. Here, we report the synthesis and crystal structure of three new complexes (**1**, **2**, and **3**), as well spectroscopic studies and DFT calculations of these three complexes along with comparisons with three other closely related thiosemicarbazones whose crystal structures have previously been published (**4** [12], **5** [13], and **6** [14]). These structures are similar in structure, but vary in the position of a methoxy group on the aryl ring, and either a methyl or ethyl group on the terminal amine nitrogen, as shown in Scheme 1 below.



Scheme 1. Synthesis of thiosemicarbazones.

The typical synthesis of thiosemicarbazones is a condensation between a ketone (or aldehyde) and a thiosemicarbazide. The crystal structures of some other closely related thiosemicarbazones, *N*-Ethyl-2-[1-(2-hydroxy-4-methylphenyl)ethylidene]hydrazinecarbothioamide [15] and *N*-Ethyl-2-[1-(2-hydroxynaphthalen-1-yl)ethylidene] hydrazinecarbothioamide [16], have also been reported.

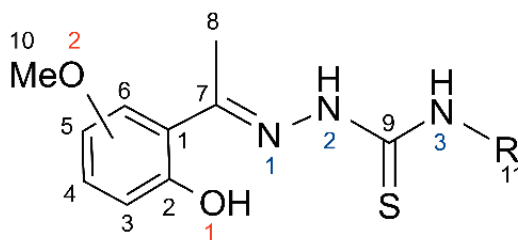
2. Results and Discussion

2.1. Structural Study of (1), (2) and (3)

In this discussion, structural and theoretical comparisons are grouped around pairs of compounds that are similar in containing a 4-methoxy, 5-methoxy or 6-methoxy substitution on the 2-hydroxy-phenyl ring and either a methyl or ethyl group on the terminal amine group, respectively, providing responses for three related pairs of compounds.

Numbering of Structures in Crystal Structure Tables

The numbering system chosen to compare the structural and theoretical data of compounds (**1**), (**2**) and (**3**) is based on the template shown below (Scheme 2). In compounds (**4**), (**5**) and (**6**), the numbering system of the published structures is translated to coincide with the new data in (**1**), (**2**) and (**3**).



Scheme 2. Numbering system for theoretical and experimental data on thiosemicarbazones.

Figure 1 below, shows the Ortep drawing and packing diagram of Compound (1): 2-[1-(2-hydroxy-5-methoxyphenyl)ethylidene]-*N*-methyl-hydrazinecarbothioamide monohydrate.

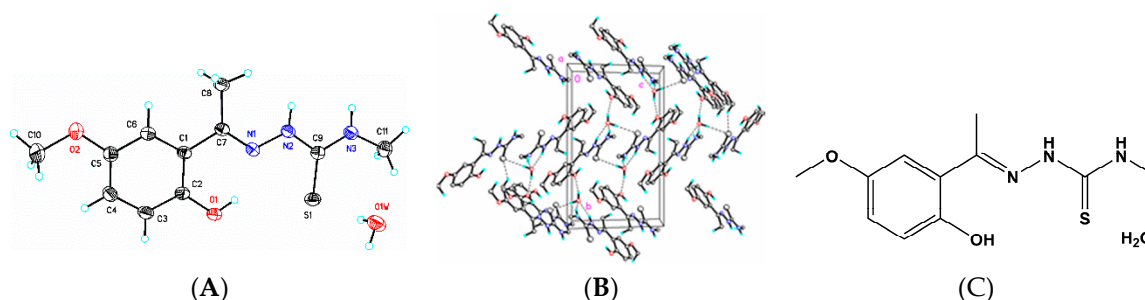


Figure 1. (A) ORTEP drawing of (1) showing the atom numbering scheme and 50% probability displacement ellipsoids of non-H atoms; (B, C) The molecular packing of (1) viewed along the *a* axis. Dashed lines indicate O–H···N, N–H···O, O–H···O intramolecular hydrogen bonds and weak C–H···S, C–H···O, O–H···S intermolecular interactions forming a 3D supramolecular structure. Hydrogen atoms not involved in hydrogen bonding have been removed for clarity.

Figure 2 below, shows the Ortep drawing and packing diagram of Compound (2): 2-[1-(2-hydroxy-5-methoxyphenyl)ethylidene]-*N*-ethyl-hydrazinecarbothioamide.

In (1), $C_{11}H_{15}N_3O_2S \cdot H_2O$, one molecule and a water molecule crystallize in the asymmetric unit, while in (2), $C_{12}H_{17}N_3O_2S$, a single molecule is present. Bond lengths and angles for both compounds are in normal ranges [17] (Table 1). In (1), the dihedral angle between the mean planes of the phenyl ring and hydrazinecarbothioamide group (N1/N2/C8/S1/N3) is $2.0(5)^\circ$, forming a nearly planar molecule. In the crystal, an N2–H2···O1W intermolecular hydrogen bond in concert with a weak O1W–H1WB···S1 intermolecular interaction along with the C9–N3 fragment form an $R_4^4(12)$ ring motif structure (Figure 1). Additional O1–H1···N1 intramolecular hydrogen bonds involving the hydroxyl group along with weak C–H···O, C–H···S and N–H···OW, OW–H···S intermolecular interactions (Table 2) are also observed forming a three-dimensional (3D) supramolecular structure.

In (2) the dihedral angle between the mean planes of the phenyl ring and hydrazinecarbothioamide group (N1/N2/C8/S1/N3) is $50.3(8)^\circ$, forming a significantly twisted molecule. In the crystal, an intramolecular O1–H1···N1 hydrogen bond forms a $R_2^2(20)$ ring motif structure (Figure 2). In addition, a weak N2–H2···S1 intermolecular interaction, which gives rise to a $R_2^2(8)$ ring motif along with a weak N3–H3···O2 interaction involving the 5-methoxy oxygen atom, forms a two-dimensional (2D) network structure (Table 2).

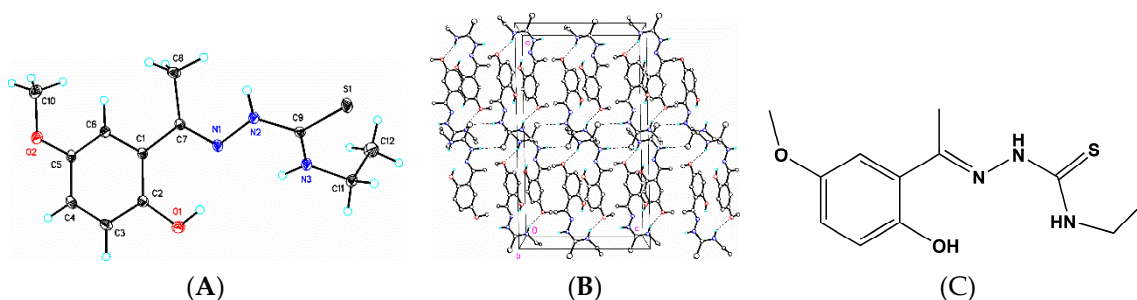


Figure 2. (A) ORTEP drawing of (2) showing the atom numbering scheme and 50% probability displacement ellipsoids of non-H atoms; (B, C) The molecular packing of (2) viewed along the *b* axis. Dashed lines indicate O–H···O intramolecular hydrogen bonds and weak N–H···S, N–H···O intermolecular interactions forming a 2D network structure. Hydrogen atoms not involved in hydrogen bonding have been removed for clarity.

Table 1. Selected crystal and DFT * bond lengths (Å), bond angles (°), and torsion angles (°): (1)–(2).

Atoms	Distance, Å	DFT, Å	Distance	DFT, Å
C1-C7	1.4783(16)	1.487 *	1.4754(14)	1.469 *
C2-O1	1.3646(15)	1.365 *	1.3555(13)	1.348 *
C5-O2	1.3660(16)	1.371 *	1.3809(13)	1.359 *
C7-N1	1.2890(16)	1.290 *	1.2995(14)	1.305 *
N2-C9	1.3626(16)	1.386 *	1.3543(13)	1.381 *
C9-S1	1.6815(13)	1.665 *	1.6903(10)	1.684 *
C9-N3	1.3334(16)	1.370 *	1.3273(13)	1.347 *
N3-C11	1.4522(18)	1.454 *	1.4565(14)	1.460 *

(1) C₁₁H₁₅N₃O₂S · H₂O

Atoms	Distance, Å	DFT, Å	Distance	DFT, Å
C1-C7-N1	115.27(10)	117.19 *	117.17(9)	117.64 *
C8-C7-N1	125.67(11)	123.90 *	123.94(9)	120.51 *
C7-N1-N2	120.44(10)	118.04 *	117.28(9)	119.41 *
N1-N2-C9	119.03(10)	122.12 *	119.67(9)	121.40 *
N2-C9-N3	113.99(11)	110.94 *	116.91(9)	115.10 *
N2-C9-S1	122.47(9)	118.63 *	119.56(8)	118.63 *

(2) C₁₂H₁₇N₃O₂S

Atoms	Distance, Å	DFT, Å	Distance	DFT, Å
C7-N1-N2-C9	−177.40(11)	173.15 *	−152.54(10)	172.86 *
C1-C7-N1-N2	178.93(10)	179.36 *	−173.28(9)	176.73 *
N1-N2-C9-N3	−177.90(10)	174.62 *	16.31(15)	−14.94 *
N1-N2-C9-S1	2.06(15)	−6.78 *	−165.17(8)	166.03 *

* DFT B3LYP 6-31 G(d) geometry optimization calculations for (1) and (2).

Table 2. Hydrogen bond interactions for (1) and (2) (Å and °).

D-H...A	d(D-H)/Å	d(H-A)/Å	d(D...A)/Å	<(DHA)/°
(1) C₁₁H₁₅N₃O₂S · H₂O				
O1-H1...N1	0.84	1.85	2.521(13)	143.7
N2-H2...O1W #1	0.88	2.07	2.8869(14)	155.0
N3-H2...O1W #1	0.88	2.23	3.0367(16)	151.4
C8-H8B...O1 #2	0.98	2.81	3.4458(17)	123.1
C10-H10A...S1 #3	0.98	2.82	3.4756(18)	124.9
C11-H11B...O2 #2	0.98	2.68	3.3833(19)	129.1
O1W-H1WA...O1 #4	0.85	1.99	2.8200(13)	165.3
O1W-H1WB...S1	0.85	2.43	3.2691(11)	167.3
(2) C₁₂H₁₇N₃O₂S				
O1-H1...N1	0.84	1.91	2.6317(12)	144.0
N2-H2...S1 #5	0.88	1.91	3.3348(9)	160.6
N3-H3...O2 #6	0.88	2.25	3.0145(12)	144.6

Symmetry Codes: #1 1 - x, 1 - y, 1 - z; #2 1 - x, 1 - y, 1 - z; #3 1 + x, 3/2 - y, -1/2 + z; #4 +x, 3/2 - y, 1/2 + z; #5 1 - x, +y, 1/2 - z; #6 3/2 - x, 1/2 - y, 1 - z.

Figure 3 below, shows the Ortep drawing and packing diagram of Compound (3): 2-[1-(2-hydroxy-4-methoxyphenyl)ethylidene]-N-ethyl-hydrazinecarbothioamide acetonitrile solvate.

In (3), C₁₂H₁₇N₃O₂S·C₂H₃N, one molecule and an acetonitrile solvent molecule crystallize in the asymmetric unit, while in (4), C₁₁H₁₅N₃O₂S, a single molecule is present [12]. Bond lengths and angles for both compounds are in normal ranges [17] (Table 3). In (3) the dihedral angle between the mean planes of the phenyl ring and hydrazinecarbothioamide group (N1/N2/C8/S1/N3) is 45.4(7)°, forming a significantly twisted molecule. In the crystal, an intramolecular O1-H1...N1 hydrogen bond forms a S₁¹ (6) graph set motif (Figure 3). Additional weak C-H...O, N-H...S intermolecular interactions and a weak N3-H3...NA1 solvent interaction (Table 3) are also observed, which help stabilize the crystal packing.

Table 3. Cont.

(4) C ₁₁ H ₁₅ N ₃ O ₂ S [12]				
Atoms	Torsions, °	DFT, °	Torsions, °	DFT, °
C7-N1-N2-C9	153.11(13)	−172.15 *	178.8(2)	−171.06 *
C1-C7-N1-N2	−173.60(11)	−176.67 *	−179.2(2)	−178.66 *
N1-N2-C9-N3	−16.0(2)	14.87 *	−177.6(2)	−176.89 *
N1-N2-C9-S1	165.79(10)	−166.08 *	2.8(3)	4.08 *

* DFT B3LYP 6-31 G(d) geometry optimization calculations for (3) and (4).

Table 4. Hydrogen bond interactions for (3) and (4) [Å and °].

D-H...A	d(D-H)/Å	d(H-A)/Å	d(D...A)/Å	<(DHA)/°
(1) C ₁₂ H ₁₇ N ₃ O ₂ S·C ₂ H ₃ N				
O1-H1...N1	0.84	1.85	2.5846(16)	145.3
N2-H2...S1 #1	0.88	2.69	3.3936(13)	137.5
N3-H3...NA1 #2	0.88	2.41	3.181(2)	145.8
C12-H12A...O2 #3	0.98	2.55	3.343(2)	137.5
C2A-H2AA...O2 #4	0.98	2.82	3.4756(18)	124.9
C2A-H2AB...O1 #2	0.98	2.68	3.3833(19)	129.1
(2) C ₁₁ H ₁₅ N ₃ O ₂ S [12]				
O1-H1...N1	0.82	1.85	2.5661(3)	145.0
C10-H10A...O2 #5	0.96	2.59	3.301(4)	132.0
C10-H10C...O1 #6	0.96	2.27	3.481(4)	158.0

Symmetry Codes: #1 2 - x, 1 - y, 1 - z; #2 2 - x, 1 - y, 2 - z; #3 1 - x, 2 - y, 3 - z; #4 + x, 1 - y, -1 + z; #5 -1/2 + x, 1/2 - y, -1/2 + z; #6 1 - x, 1 - y, 1 - z.

Compound (5): 2-[1-(2-hydroxy-6-methoxyphenyl)ethylidene]-N-methyl-hydrazinecarbothioamide acetonitrile monosolvate [13].

In (5), C₁₁H₁₅N₃O₂S·C₂H₃N, one molecule and an acetonitrile solvent molecule crystallize in the asymmetric unit [13], while in (6), C₁₂H₁₇N₃O₂S, a single molecule is present [14]. Bond lengths and angles for both compounds are in normal ranges [17] (Table 5). In (5) the dihedral angle between the mean planes of the phenyl ring and hydrazinecarbothioamide group (N1/N2/C8/S1/N3) is 75.1(2)° forming a significantly twisted molecule (Figure 5) [13]. In the crystal, the main molecule is linked to the solvent molecule by a weak N-H...N hydrogen bond while O-H...S hydrogen bonds (Table 6) link the molecules into columns along [100].

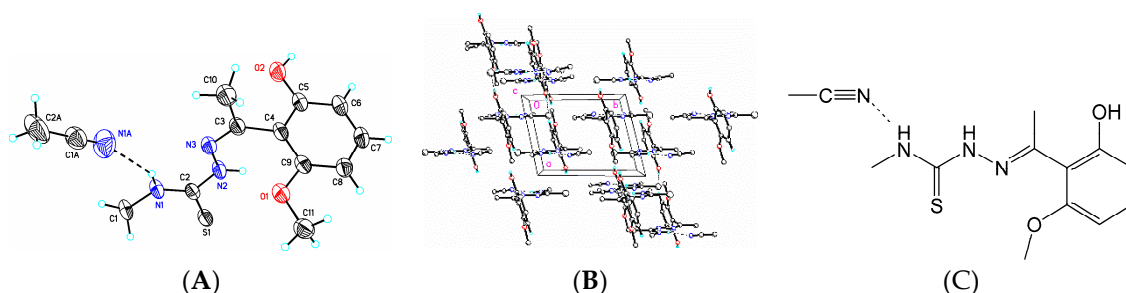


Figure 5. (A) ORTEP drawing of (5) showing the atom numbering scheme and 50% probability displacement ellipsoids of non-H atoms; (B, C) The molecular packing for (5) viewed along the *b* axis. Dashed lines indicate N-H...N intramolecular hydrogen bonds and weak O-H...S intermolecular interactions. Hydrogen atoms not involved in hydrogen bonding have been removed for clarity.

Compound (6): 2-[1-(2-hydroxy-6-methoxyphenyl)ethylidene]-N-ethyl-hydrazinecarbothioamide [14].

In (6) the dihedral angle between the mean planes of the phenyl ring and hydrazinecarbothioamide group (N1/N2/C8/S1/N3) is 86.8(4)° also forming a significantly

twisted molecule (Figure 6) [14]. In the crystal, intermolecular O–H \cdots S hydrogen bonds (Table 6) link the molecules into chains along [001].

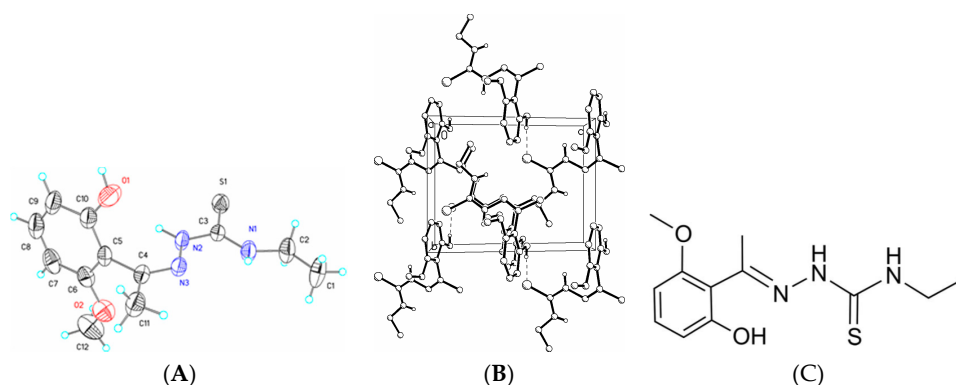


Figure 6. (A) ORTEP drawing of (6) showing the atom numbering scheme and 50% probability displacement ellipsoids of non-H atoms; (B, C) The molecular packing of (6) viewed along the *b* axis. Dashed lines indicate weak O–H \cdots S intermolecular interactions. Hydrogen atoms not involved in hydrogen bonding have been removed for clarity.

Table 5. Selected crystal and DFT* bond lengths (Å), bond angles (°), and torsion angles (°): (5)–(6).

Atoms	Distance, Å	DFT, Å	Distance	DFT, Å
C1–C7	1.495(3)	1.498 *	1.487(3)	1.498 *
C2–O1	1.361(3)	1.368 *	1.367(3)	1.365 *
C6–O2	1.371(3)	1.360 *	1.362(3)	1.363 *
C7–N1	1.278(3)	1.288 *	1.281(3)	1.298 *
N2–C9	1.357(3)	1.375 *	1.355(3)	1.376 *
C9–S1	1.692(2)	1.684 *	1.688(2)	1.685 *
C9–N3	1.327(3)	1.345 *	1.311(3)	1.344 *
N3–C11	1.453(3)	1.451 *	1.471(3)	1.456 *
(5) C₁₁H₁₅N₃O₂S·C₂H₃N [13]				
Atoms	Angles, °	DFT, °	Angles, °	DFT, °
C1–C7–N1	124.78(19)	124.40 *	124.46(19)	124.26 *
C8–C7–N1	117.49(19)	117.42 *	117.74(18)	117.51 *
C7–N1–N2	117.10(17)	119.46 *	116.48(17)	119.33 *
N1–N2–C9	119.82(17)	121.33 *	119.04(16)	121.32 *
N2–C9–N3	116.28(19)	114.89 *	116.6(2)	114.96 *
N2–C9–S1	119.40(16)	119.79 *	119.71(15)	119.59 *
(6) C₁₂H₁₇N₃O₂S [14]				
Atoms	Angles, °	DFT, °	Angles, °	DFT, °
C7–N1–N2–C9	−175.26(18)	178.25 *	178.22(19)	178.32 *
C1–C7–N1–N2	3.1(3)	−1.06 *	−0.6(3)	−1.98 *
N1–N2–C9–N3	−1.7(3)	0.68 *	1.3(3)	0.35 *
N1–N2–C9–S1	178.38(18)	−179.17 *	−179.12(15)	−179.62 *

* DFT B3LYP 6-31 G(d) geometry optimization calculations for (5) and (6).

Table 6. Hydrogen bond interactions for (5) and (6) [Å and °].

D–H ... A	d(D–H)/Å	d(H–A)/Å	d(D \cdots A)/Å	<(DHA)/°
(1) C₁₁H₁₅N₃O₂S·C₂H₃N [13]				
O2–H2 \cdots S1 #1	0.84	2.34	3.1823(17)	177.0
N1–H1 \cdots N1A	0.88	2.25	3.039(3)	149.0
(2) C₁₂H₁₇N₃O₂S [14]				
O1–H1 \cdots S1 #2	0.82	2.35	3.1655(19)	175.0

Symmetry Codes: #1 – *x*, – *y* + 2, 2 – *z*; #2 *x*, –*y*, 1/2 + *z*.

2.2. Theoretical Study of (1) and (2)

After a DFT geometry optimization calculation for (1), the dihedral angle between the mean planes of the phenyl ring and hydrazinecarbothioamide group (N1/N2/C8/S1/N3) becomes $54.4(9)^\circ$, an increase of $52.4(4)^\circ$. Bond lengths, bond angles and torsion angles show only small changes (Table 1). However, the large increase in the angle between the mean planes of the phenyl ring and hydrazinecarbothioamide group suggests that the influence of the water molecule and numerous intra- and intermolecular interactions is significant. The N2–H2 \cdots O1W intermolecular hydrogen bond in concert with a weak O1W–H1WB \cdots S1 and additional O1–H1 \cdots N1 intramolecular hydrogen bonds involving the hydroxyl group along weak C–H \cdots O, C–H \cdots S and N–H \cdots OW, OW–H \cdots S intermolecular interactions (Table 2) obviously play a role in this observation and in the crystal packing of the molecule.

After a DFT geometry optimization calculation for (2), the dihedral angle between the mean planes of the phenyl ring and hydrazinecarbothioamide group (N1/N2/C8/S1/N3) becomes $24.5(5)^\circ$, a decrease of $25.8(4)^\circ$. Bond lengths, bond angles and torsion angles show only small changes (Table 1). However, the large decrease in the angle between the mean planes of the phenyl ring and hydrazinecarbothioamide group suggests that the influence of the numerous intra- and intermolecular interactions is significant. The weak N2–H2 \cdots S1, N3–H3 \cdots O2 intermolecular interactions in concert with the O1–H1 \cdots N1 intramolecular hydrogen bond (Table 2) appear to play a role in these observations and in the crystal packing of the molecule.

Calculated molecular orbital energies (eV) for the surfaces of the frontier molecular orbitals for (1) show three absorption band envelopes, exhibiting some blue shifts, which are consistent with the experimental data (Figure 7 and Table 7) with λ_{max} values located at 217, 297, and 348 nm, respectively. The bands in the UV region, 215–350 nm, are assigned to $n \rightarrow \pi^*$, $\pi \rightarrow \pi^*$ and $n \rightarrow n^*$ transitions. In the Highest Occupied Molecular Orbital (HOMO) the electronic clouds are distributed primarily on the sulfur atom. In HOMO–1 they are located on the phenyl ring and the hydrazinecarbothioamide group. In Lowest Unoccupied Molecular Orbital (LUMO) and LUMO+1 the electronic clouds are delocalized primarily on the phenyl ring while in LUMO+2 they are dispersed on both the hydrazinecarbothioamide group and phenyl ring. Therefore, the first absorption band envelope at 348 nm is assigned to contributions primarily from HOMO \rightarrow LUMO and HOMO–1 \rightarrow LUMO. The second absorption band at 297 nm is assigned to overlapping contributions from HOMO \rightarrow LUMO+1 and HOMO–1 \rightarrow LUMO+1. The third absorption band at 217 nm is assigned to overlapping contributions from HOMO \rightarrow LUMO+2 and HOMO–1 \rightarrow LUMO+2, respectively. It is evident that electron transitions among frontier molecular orbitals in (1) are corresponding to $n \rightarrow \pi^*$, $\pi \rightarrow \pi^*$ and $n \rightarrow n^*$ transitions.

Calculated molecular orbital energies (eV) for the surfaces of the frontier molecular orbitals for (2) show three absorption band envelopes, exhibiting some blue shifts, which are consistent with the experimental data (Figure 7 and Table 7) with λ_{max} values located at 207, 296, and 346 nm, respectively. The bands in the UV region, 200–350 nm, are assigned to $n \rightarrow \pi^*$, $\pi \rightarrow \pi^*$ and $\pi \rightarrow n^*$ transitions. In HOMO the electronic clouds are distributed primarily on the phenyl ring. In HOMO–1 they are located on the phenyl ring and the hydrazinecarbothioamide group. In LUMO, LUMO+1 and LUMO+2 the electronic clouds are dispersed on both the hydrazinecarbothioamide group and phenyl ring. Therefore, the first absorption band envelope at 346 nm is assigned to contributions primarily from HOMO \rightarrow LUMO. The second absorption band at 296 nm is assigned to HOMO–1 \rightarrow LUMO. The third absorption band at 207 nm is assigned to overlapping contributions from HOMO \rightarrow LUMO+1, HOMO–1 \rightarrow LUMO+1, HOMO \rightarrow LUMO+2 and HOMO–1 \rightarrow LUMO+2, respectively. It is evident that electron transitions among frontier molecular orbitals in (2) are corresponding to $n \rightarrow \pi^*$, $\pi \rightarrow \pi^*$ and $\pi \rightarrow n^*$ transitions.

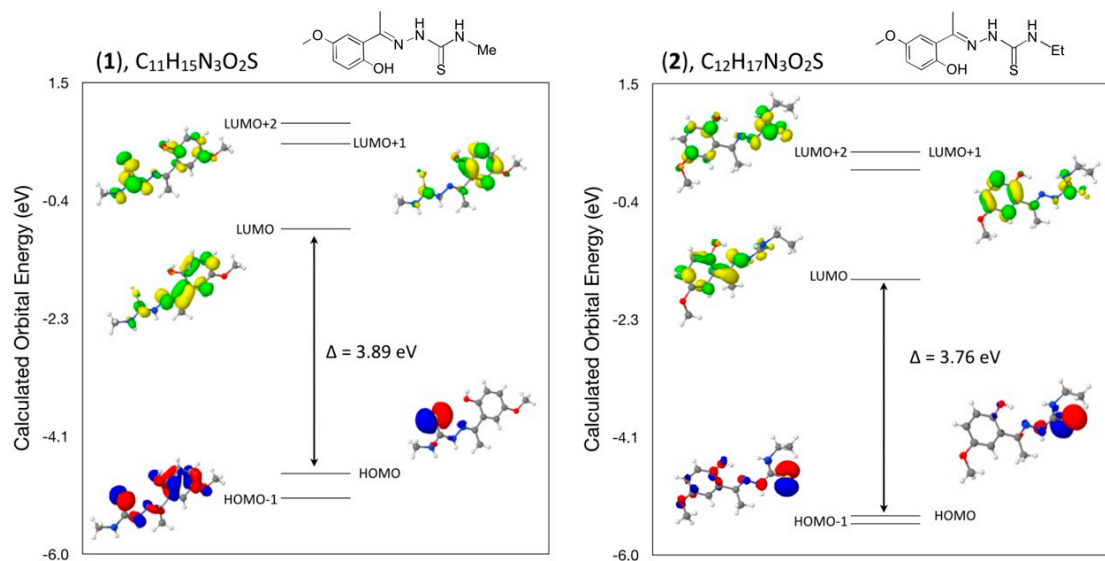


Figure 7. Calculated frontier molecular orbitals for $C_{11}H_{15}N_3O_2S$ (1) and $C_{12}H_{17}N_3O_2S$ (2).

Table 7. Experimental and calculated energy of molecular orbitals of (1) and (2) and associated transitions.

(1) $C_{11}H_{15}N_3O_2S$			(2) $C_{12}H_{17}N_3O_2S$		
Experimental λ (nm/eV)	Calculated λ (nm/eV)	MO Contribution	Experimental λ (nm/eV)	Calculated λ (nm/eV)	MO Contribution
348/3.52	318.7/3.89	HOMO→LUMO	346/3.58	329.8/3.76	HOMO→LUMO
348/3.52	289.5/4.28	HOMO-1→LUMO	296/4.19	319.3/3.88	HOMO-1→LUMO
297/4.17	236.2/5.25	HOMO→LUMO+1	201/6.17	224.9/5.51	HOMO→LUMO+1
297/4.17	222.4/5.57	HOMO-1→LUMO+1	201/6.17	220.0/5.64	HOMO-1→LUMO+1
217/5.71	219.7/5.64	HOMO→LUMO+2	201/6.17	213.9/5.79	HOMO→LUMO+2
217/5.71	207.7/5.97	HOMO-1→LUMO+2	201/6.17	209.5/5.98	HOMO-1→LUMO+2

2.3. Theoretical Study of (3) and (4)

After a DFT geometry optimization calculation for (3), the dihedral angle between the mean planes of the phenyl ring and hydrazinecarbothioamide group (N1/N2/C8/S1/N3) becomes $22.7(7)^\circ$, a decrease of $22.8(0)^\circ$. Bond lengths, bond angles and torsion angles show only small changes (Table 3). However, the small decrease in the angle between the mean planes of the phenyl ring and hydrazinecarbothioamide group suggests that the influence of the numerous intra- and intermolecular interactions is significant. The weak $N2-H2 \cdots S1$, $C12-H12A \cdots O2$, $C2A-H2AA \cdots O2$, $C2A-H2AB \cdots O1$ intermolecular interactions in concert with a weak $N3-H3 \cdots NA1$ solvent interaction along with an $O1-H1 \cdots N1$ intramolecular hydrogen bond (Table 4) appear to play a role in these observations and in the crystal packing of the molecule.

After a DFT geometry optimization calculation for (4), the dihedral angle between the mean planes of the phenyl ring and hydrazinecarbothioamide group (N1/N2/C8/S1/N3) becomes $4.5(0)^\circ$, a decrease of $4.7(1)^\circ$. Bond lengths, bond angles and torsion angles show only small changes (Table 3). The small decrease in the angle between the mean planes of the phenyl ring and hydrazinecarbothioamide group suggests that the influence of the one intra- and two intermolecular interactions is involved. The weak $C10-H10A \cdots O2$, $C10-H10A \cdots O1$ intermolecular interactions along with an $O1-H1 \cdots N1$ intramolecular hydrogen bond (Table 4) appear to play a role in these observations and in the crystal packing of the molecule.

Calculated molecular orbital energies (eV) for the surfaces of the frontier molecular orbitals for (3) show three absorption band envelopes, exhibiting some blue shifts, which are consistent with the experimental data (Figure 8 and Table 8) with λ_{max} values located at 207, 241 and 329 nm, respectively.

The bands in the UV region, 255–330 nm, are assigned to $n \rightarrow \pi^*$, $\pi \rightarrow \pi^*$ and $n \rightarrow n^*$ transitions. In HOMO and HOMO–1 the electronic clouds are distributed primarily on the hydrazinecarbothioamide group. In LUMO they are located on the phenyl ring and hydrazinecarbothioamide group. In LUMO+1 the electronic clouds are delocalized primarily on the phenyl ring while in LUMO+2 they are dispersed on the hydrazinecarbothioamide group. Therefore, the first absorption band envelope at 329 nm is assigned to contributions primarily from HOMO→LUMO and HOMO–1→LUMO. The second absorption band at 241 nm is assigned to HOMO→LUMO+1 and HOMO–1→LUMO+1. The third absorption band envelope at 207 nm is assigned to overlapping contributions from HOMO→LUMO+2 and HOMO–1→LUMO+2, respectively. It is evident that electron transitions among frontier molecular orbitals in (3) are corresponding to $n \rightarrow \pi^*$, $\pi \rightarrow \pi^*$ and $n \rightarrow n^*$ transitions.

Calculated molecular orbital energies (eV) for the surfaces of the frontier molecular orbitals for (4) show four absorption band envelopes, exhibiting some blue shifts, which are consistent with the experimental data (Figure 8 and Table 8) with λ_{\max} values located at 208, 242, 298, and 332 nm, respectively. The bands in the UV region, 255–340 nm, are assigned to $n \rightarrow \pi^*$, $\pi \rightarrow \pi^*$ and $n \rightarrow n^*$ transitions. In HOMO the electronic clouds are distributed primarily on the sulfur atom. In HOMO–1 and LUMO they are located on the phenyl ring and the hydrazinecarbothioamide group. In LUMO+1 the electronic clouds are delocalized primarily on the phenyl ring while in LUMO+2 they are dispersed on the hydrazinecarbothioamide group. Therefore, the first absorption band envelope at 332 nm is assigned to contributions primarily from HOMO→LUMO. The second absorption band at 297 nm is assigned to HOMO–1→LUMO. The third absorption band envelope at 242 nm is assigned to overlapping contributions from HOMO→LUMO+1, HOMO–1→LUMO+1 and HOMO→LUMO+2, respectively, while the fourth absorption band is assigned to HOMO–1→LUMO+2. It is evident that electron transitions among frontier molecular orbitals in (4) are corresponding to $n \rightarrow \pi^*$, $\pi \rightarrow \pi^*$ and $n \rightarrow n^*$ transitions.

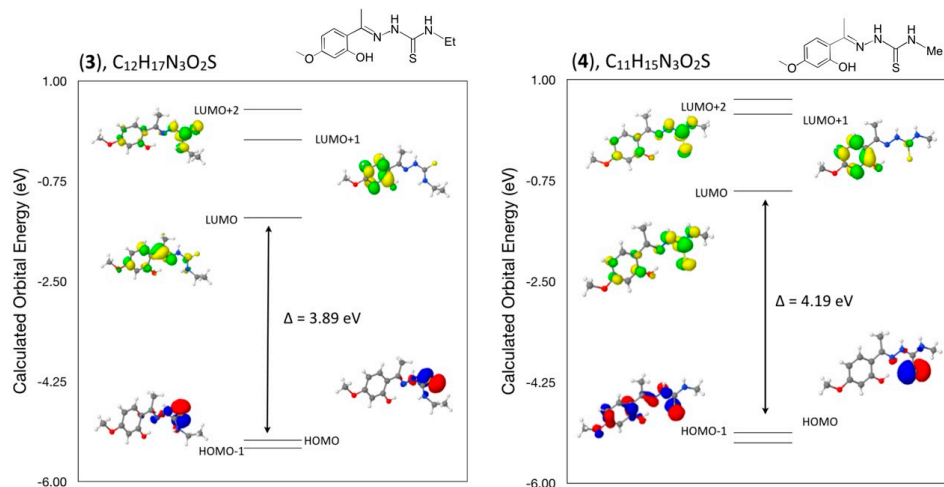


Figure 8. Calculated frontier molecular orbitals for $C_{12}H_{17}N_3O_2S$ (3) and $C_{11}H_{15}N_3O_2S$ (4).

Table 8. Experimental and calculated energy of molecular orbitals of (3) and (4) and associated transitions.

(3) $C_{12}H_{17}N_3O_2S$			(4) $C_{11}H_{15}N_3O_2S$		
Experimental λ (nm/eV)	Calculated λ (nm/eV)	MO Contribution	Experimental λ (nm/eV)	Calculated λ (nm/eV)	MO Contribution
329/3.77	318.9/3.89	HOMO→LUMO	332.3/3.73	295.8/4.19	HOMO→LUMO
329/3.77	307.8/4.02	HOMO–1→LUMO	298.6/4.15	283.4/4.37	HOMO–1→LUMO
241/5.14	236.3/5.25	HOMO→LUMO+1	242/5.12	224.6/5.52	HOMO→LUMO+1
241/5.14	230.1/5.39	HOMO–1→LUMO+1	242/5.12	217.4/5.70	HOMO–1→LUMO+1
207/5.99	214.7/5.77	HOMO→LUMO+2	242/5.12	214.5/5.78	HOMO→LUMO+2
207/5.99	209.6/5.91	HOMO–1→LUMO+2	208/5.96	207.9/5.96	HOMO–1→LUMO+2

2.4. Theoretical Study of (5) and (6)

After a DFT geometry optimization calculation for (5), the dihedral angle between the mean planes of the phenyl ring and hydrazinecarbothioamide group (N1/N2/C8/S1/N3) becomes $68.5(7)^\circ$, a decrease of $6.5(5)^\circ$. Bond lengths, bond angles and torsion angles show only small changes (Table 5). The small decrease in the angle between the mean planes of the phenyl ring and hydrazinecarbothioamide group suggests that the influence of the numerous intra- and intermolecular interactions is small. The weak O2–H2 \cdots S1 intermolecular interactions along with a N1–H1 \cdots NA1 solvent interaction (Table 6) appear to play a role in these observations and in the crystal packing of the molecule.

After a DFT geometry optimization calculation for (6), the dihedral angle between the mean planes of the phenyl ring and hydrazinecarbothioamide group (N1/N2/C8/S1/N3) becomes $70.8(0)^\circ$, a decrease of $16.0(4)^\circ$. Bond lengths, bond angles and torsion angles show only small changes (Table 5). The moderate decrease in the angle between the mean planes of the phenyl ring and hydrazinecarbothioamide group suggests that the influence of the weak O2–H2 \cdots S1 intermolecular interactions is small (Table 6) and appears to play a small role in these observations and in the crystal packing of the molecule.

Calculated molecular orbital energies (eV) for the surfaces of the frontier molecular orbitals for (5) show three absorption band envelopes, exhibiting some blue shifts, which are consistent with the experimental data (Figure 9 and Table 9) with λ_{\max} values located at 203, 240 and 273 nm, respectively. The bands in the UV region, 20–275 nm, are assigned to $n \rightarrow \pi^*$, $\pi \rightarrow \pi^*$ and $n \rightarrow n^*$ transitions. In HOMO and HOMO–1 the electronic clouds are distributed primarily on the hydrazinecarbothioamide group. In LUMO and LUMO+1 they are located on the phenyl ring and hydrazinecarbothioamide group. In LUMO+2 the electronic clouds are delocalized primarily on the phenyl ring. Therefore, the first absorption band envelope at 273 nm is assigned to contributions primarily from HOMO \rightarrow LUMO and HOMO–1 \rightarrow LUMO. The second absorption band at 240 nm is assigned to HOMO \rightarrow LUMO+1 and HOMO–1 \rightarrow LUMO+1. The third absorption band envelope at 203 nm is assigned to overlapping contributions from HOMO \rightarrow LUMO+2 and HOMO–1 \rightarrow LUMO+2, respectively. It is evident that electron transitions among frontier molecular orbitals in (5) are corresponding to $n \rightarrow \pi^*$, $\pi \rightarrow \pi^*$ and $n \rightarrow n^*$ transitions.

Calculated molecular orbital energies (eV) for the surfaces of the frontier molecular orbitals for (6) show three absorption band envelopes, exhibiting some blue shifts, which are consistent with the experimental data (Figure 9 and Table 9) with λ_{\max} values located at 197, 239 and 275 nm, respectively. The bands in the UV region, 185–280 nm, are assigned to $n \rightarrow \pi^*$, $\pi \rightarrow \pi^*$ and $n \rightarrow n^*$ transitions. In HOMO and HOMO–1 the electronic clouds are distributed primarily on the hydrazinecarbothioamide group. In LUMO and LUMO + 2 they are located on the phenyl ring. In LUMO+1 the electronic clouds are delocalized primarily on the hydrazinecarbothioamide group. Therefore, the first absorption band envelope at 275 nm is assigned to contributions primarily from HOMO \rightarrow LUMO. The second absorption band at 239 nm is assigned to HOMO–1 \rightarrow LUMO. The third absorption band envelope at 197 nm is assigned to overlapping contributions from HOMO \rightarrow LUMO+1, HOMO–1 \rightarrow LUMO+1, HOMO \rightarrow LUMO+2 and HOMO–1 \rightarrow LUMO+2, respectively. It is evident that electron transitions among frontier molecular orbitals in (6) are corresponding to $n \rightarrow \pi^*$, $\pi \rightarrow \pi^*$ and $n \rightarrow n^*$ transitions.

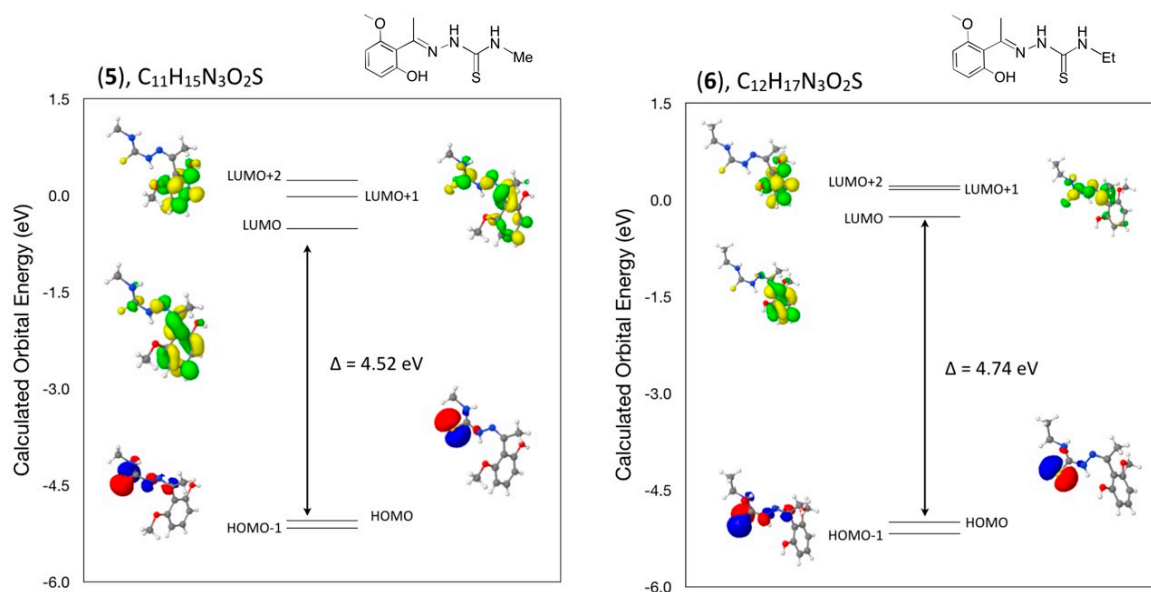


Figure 9. Calculated frontier molecular orbitals for $C_{11}H_{15}N_3O_2S$ (5) and $C_{12}H_{17}N_3O_2S$ (6).

Table 9. Experimental and calculated energy of molecular orbitals of (5) and (6) and associated transitions.

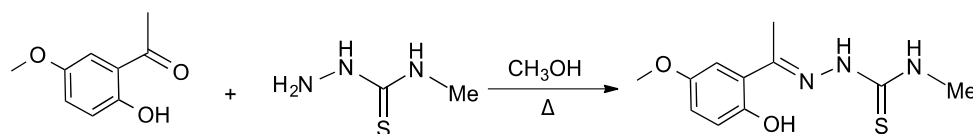
(5) $C_{11}H_{15}N_3O_2S$			(6) $C_{12}H_{17}N_3O_2S$		
Experimental λ (nm/eV)	Calculated λ (nm/eV)	MO Contribution	Experimental λ (nm/eV)	Calculated λ (nm/eV)	MO Contribution
273/4.54	273.8/4.52	HOMO→LUMO	275/4.51	261.7/4.74	HOMO→LUMO
273/4.54	266.7/4.65	HOMO-1→LUMO	239/5.19	252.5/4.91	HOMO-1→LUMO
240/5.17	246.5/5.03	HOMO→LUMO+1	197/6.29	240.2/5.16	HOMO→LUMO+1
240/5.17	240.7/5.15	HOMO-1→LUMO+1	197/6.29	238.1/5.21	HOMO-1→LUMO+1
203/6.11	234.8/5.28	HOMO→LUMO+2	197/6.29	232.3/5.34	HOMO→LUMO+2
203/6.11	229.5/5.40	HOMO-1→LUMO+2	197/6.29	230.3/5.38	HOMO-1→LUMO+2

3. Experimental Procedures

3.1. General Information for the Synthesis of Compounds (1)–(6)

All reagents were purchased from Sigma Aldrich Co., St Louis, MS, USA. NMR spectra were obtained using a JEOL ECS-400 MHz spectrometer at room temperature unless otherwise stated. Chemical shifts are reported in ppm and referenced via residual solvent resonances to Me_4Si (1H and ^{13}C). Melting points were taken in open capillary tubes and are uncorrected. Absorption spectra were recorded in acetonitrile (from 6×10^{-4} to 2×10^{-5} M at room temperature) on a Cary 300 UV-Vis spectrophotometer. NMR (Figure S1–S12) and UV-Vis spectra (Figure S13–S18) for all compounds can be found in the Supplementary Information.

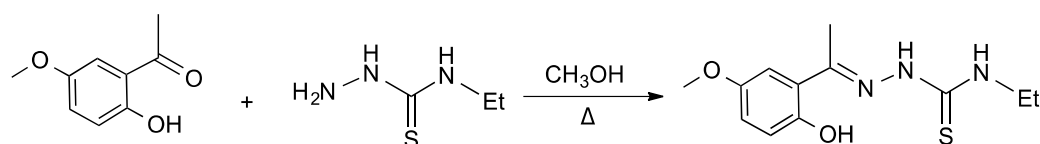
3.2. Synthesis and Spectroscopic Analysis of 2-[1-(2-Hydroxy-5-Methoxyphenyl)Ethylidene]-N-Methyl-Hydrazinecarbothioamide (1)



A 25 mL round bottom flask was charged with 5 mL of 1:1 mixture of ethanol: deionized water solution and then 0.2 g (1 equiv) of starting ketone and 0.17 g (1 equiv) of the thiosemicarbazide were added. The solution was refluxed for 48 h, after dichloromethane (5 mL) and deionized water

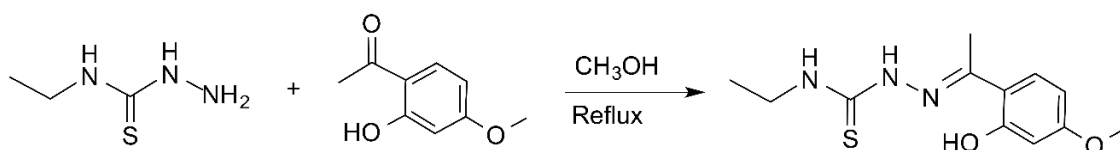
(5 mL) were added, and the organic layer was separated. The aqueous layer was then extracted with an additional 5 mL of dichloromethane, the organic layers were combined, washed with brine (2 × 5 mL), dried with magnesium sulfate, and the solvent removed *in vacuo*. The resulting product was crystallized from acetonitrile or dichloromethane layered with hexanes in 58% yield. M.p. 399–402 K. ¹H NMR (acetone-*d*₆, δ): 11.7 (br s, 1H, NH), 9.52 (br s, 1H, OH), 7.73 (br s, 1H, NH), 7.5 (d, *J* = 8.6 Hz, 1H, Ar), 6.47 (d, *J* = 8.6 Hz, 1H, Ar), 6.42 (d, 1H, Ar), 3.80 (s, 3H, CH₃), 3.13 (d, *J* = 4.7 Hz, 3H, CH₃), 2.43 (s, 3H, CH₃). ¹³C {¹H} NMR (acetone-*d*₆, δ): 180.4 (C=S), 162.3 (C=N), 160.1 (Ar), 155.1 (Ar), 129.9 (Ar), 113.5 (Ar), 105.9 (Ar), 101.5 (Ar), 54.9 (OMe), 29.6 (Me), 13.6 (Me).

3.3. Synthesis and Spectroscopic Analysis of 2-[1-(2-Hydroxy-5-Methoxyphenyl)Ethylidene]-*N*-Ethyl-Hydrazinecarbothioamide (2)



A 50 mL round bottom flask was charged with 2'-hydroxy-4'-methoxyacetophenone (0.206 g, 1.24 mmol), and 4-ethyl-3-thiosemicarbazide (0.148 g, 1.24 mmol), 20 mL of methanol and one drop of concentrated sulfuric acid. The colorless solution was then refluxed for 24 h, after which time the resulting yellow solution was transferred to a 125 mL glass separatory funnel and dichloromethane (15 mL) and water (15 mL) were added. The layers were separated and the aqueous layer was extracted with an additional 10 mL of dichloromethane. The organic layer (top) was removed, the aqueous layer was extracted with an additional 10 mL, the organic layers were combined and washed with brine (15 mL), dried with magnesium sulfate, and the solvent was removed *in vacuo*. The resulting yellow solid was recrystallized from minimal hot acetonitrile and allowed to cool to room temperature yielding yellow crystals (0.260 g, 78%). M.p. 411–416 K. ¹H NMR (acetone-*d*₆, δ): 10.6 (br s, 1H, OH), 9.50 (br s, 1H, NH), 7.83 (br s, 1H, NH), 7.05 (d, *J* = 3 Hz, 1H, Ar), 6.87 (dd, *J* = 9, 3 Hz, 1H, Ar), 6.80 (d, *J* = 9 Hz, 1H, Ar), 3.74 (s, 3H, OCH₃), 3.69 (m, 2H, CH₂CH₃), 2.42 (s, 3H, CH₃), 1.19 (t, *J* = 8 Hz, 3H, CH₂CH₃). ¹³C {¹H} NMR (acetone-*d*₆, δ): 179.5 (C=S), 152.6 (C=N), 152.4 (Ar), 151.6 (Ar), 121.5 (Ar), 117.7 (Ar), 117.0 (Ar), 113.2 (Ar), 55.187 (OMe), 39.2 (Me), 13.9, 13.8.

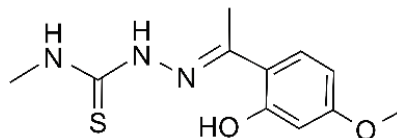
3.4. Synthesis and Spectroscopic Analysis of 2-[1-(2-Hydroxy-4-Methoxyphenyl)Ethylidene]-*N*-Ethyl-Hydrazinecarbothioamide (3)



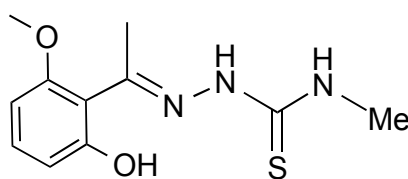
A 50 mL round bottom flask was charged with 2'-hydroxy-4'-methoxyacetophenone (0.206 g, 1.24 mmol), and 4-ethyl-3-thiosemicarbazide (0.148 g, 1.24 mmol), 20 mL of methanol and one drop of concentrated sulfuric acid. The colorless solution was then refluxed for 24 h, after which time the resulting yellow solution was transferred to a 125 mL glass separatory funnel and dichloromethane (15 mL) and water (15 mL) were added. The layers were separated and the aqueous layer was extracted with an additional 10 mL of dichloromethane. The organic layer (top) was removed, the aqueous layer was extracted with an additional 10 mL, the organic layers were combined and washed with brine (15 mL), dried with magnesium sulfate, and the solvent was removed *in vacuo*. The resulting yellow solid was recrystallized from minimal hot acetonitrile and allowed to cool to room temperature yielding yellow crystals (0.260 g, 78%). M.p. 418–420 K. ¹H NMR (CDCl₃, δ): 11.20 (s, 1H, NH), 8.54 (s, 1H, OH), 7.35 (d, *J* = 7 Hz, 1H, Ar), 6.65 (br s, 1H, NH), 6.50–6.46 (m, 2H, Ar), 3.81 (s, 3H, CH₃), 3.80–3.68 (m, 2H, CH₂), 2.33 (s, 3H, CH₃), 1.28 (t, *J* = 7 Hz, 3H, CH₃). ¹³C {¹H} NMR (acetone-*d*₆, δ):

179.5 (C=S), 162.3 (C=N), 160.1 (Ar), 154.9 (Ar), 129.9 (Ar), 113.5 (Ar), 105.9 (Ar), 101.5 (Ar), 54.9 (OMe), 39.3 (Me), 13.8, 13.5.

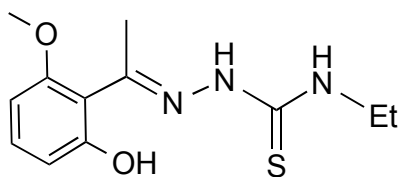
3.5. Spectroscopic Data for Compounds (4), (5), and (6)



Compound 4: ^1H NMR (acetone- d_6 , δ): 11.7 (br s, 1H, NH), 9.52 (br s, 1H, OH), 7.73 (br s, 1H, NH), 7.5 (d, $J = 8.6$ Hz, 1H, Ar), 6.47 (d, $J = 8.6$ Hz, 1H, Ar), 6.42 (d, 1H, Ar), 3.80 (s, 3H, CH_3), 3.13 (d, $J = 4.7$ Hz, 3H, CH_3), 2.43 (s, 3H, CH_3). ^{13}C $\{^1\text{H}\}$ NMR (acetone- d_6 , δ): 180.4 (C=S), 162.3 (C=N), 160.1 (Ar), 155.1 (Ar), 129.9 (Ar), 113.5 (Ar), 105.9 (Ar), 101.5 (Ar), 54.9 (OMe), 29.6 (Me), 13.6 (Me). M.p. 448–453 K.



Compound 5: ^1H NMR (acetone- d_6 , δ): 8.9 (br, 1H, NH), 8.23 (br, 1H, OH), 8.03 (br, 1H, NH), 7.25 (t, $J = 8$ Hz, 1H, Ar), 6.62 (d, $J = 8$ Hz, 2H, Ar), 3.78 (3H, OMe), 3.08 (d, $J = 4$ Hz, 3H, NMe), 2.11 (3H, Me). ^{13}C $\{^1\text{H}\}$ NMR (acetone- d_6 , δ): 178.9 (C=S), 157.2 (C=N), 154.5 (Ar), 145.3 (Ar), 131.5 (Ar), 109.4 (Ar), 108.9 (Ar), 102.9 (Ar), 55.4 (OMe), 30.5 (Me), 22.7 (Me). M.p. 415–420 K.



Compound 6: ^1H NMR (acetone- d_6 , δ): 8.97 (br, 1H, NH), 8.18 (br, 1H, OH), 8.04 (br, 1H, NH), 7.25 (t, $J = 8$ Hz, 1H, Ar), 6.64 (d, $J = 8$ Hz, 2H, Ar), 3.78 (3H, OMe), 3.67–3.60 (m, 2H, CH_2CH_3), 2.11 (3H, Me), 1.18 (t, $J = 7$ Hz, CH_2CH_3 , 3H). ^{13}C $\{^1\text{H}\}$ NMR (acetone- d_6 , δ): 177.8 (C=S), 157.2 (C=N), 154.5 (Ar), 145.4 (Ar), 131.5 (Ar), 109.3 (Ar), 108.8 (Ar), 102.9 (Ar), 55.4 (OMe), 38.8 (Me), 22.6, 14.0. M.p. 458–460 K.

3.6. X-Ray Structure Analysis and Refinement

Individual crystals of compounds (1), (2) and (3) were mounted on a CryoLoop (Hampton Research, 34 Journey, Aliso Viejo, CA, USA) and placed in a -100 °C compressed air stream on an Agilent Gemini-EOS Single Crystal Autodiffractometer at Keene State College (Agilent Technologies, LTD, Yarnton, England, Keene, NH, USA). Crystallographic data were collected using graphite monochromated 0.71073 Å Mo- $\text{K}\alpha$ radiation and integrated and corrected for absorption using the CrysAlisRed (Oxford Diffraction, 2010 software package) [18]. The structures were solved using direct methods and refined using least-square methods on F-squared [19]. The hydrogen atoms were placed in their calculated positions and included in the refinement using the riding model. All other pertinent crystallographic details such as h, k, l ranges, 2θ ranges, and R-factors can be found in Table 10.

Crystallographic Data for (1), (2) and (3)

Table 10. Crystal and experimental data for (1), (2) and (3).

Compound	1	2	3
Formula	C ₁₁ H ₁₅ N ₃ O ₂ S · H ₂ O	C ₁₂ H ₁₇ N ₃ O ₂ S	C ₁₂ H ₁₇ N ₃ O ₂ S · C ₂ H ₃ N
Formula weight	271.33	267.34	308.40
Crystal color, habit	Colorless, block	Colorless, irregular	Colorless, irregular
Crystal size (mm)	0.46 × 0.22 × 0.14	0.36 × 0.32 × 0.26	0.45 × 0.38 × 0.32
Crystal system	Monoclinic	Monoclinic	Triclinic
Space Group, Z	P2 ₁ /c, 4	C2/c, 8	P-1, 2
Temperature, K	173(s)	173(2)	173 (2)
<i>a</i> (Å)	8.2304(3)	23.3083(6)	8.9384(7)
<i>b</i> (Å)	16.2787(6)	8.2956(2)	9.5167(8)
<i>c</i> (Å)	9.9708(4)	13.5312(3)	10.0574(8)
α (°)	90	90	110.773(7)
β (°)	103.355(4)	91.077(2)	92.413(6)
γ (°)	90	90	90.654(7)
Volume, Å ³	1299.77(9)	2615.87(12)	798.89(12)
<i>F</i> (0,0,0)	576.0	1136.0	328.0
<i>m</i> (mm ⁻¹)	0.254	0.246	0.213
Q _{calc} (Mg m ⁻³)	1.387	1.358	1.282
Radiation	Mo Kα (λ = 0.7107)	Mo Kα (λ = 0.7107)	Mo Kα (λ = 0.7107)
2θ range for data collection	6.318 to 65.744°	6.036 to 65.736°	6.14 to 65.516°
Reflections collected	15566	16344	9837
Independent Reflections/R _{int}	4479/0.0343	4463/0.0353	5259/0.0379
Data/restraints/parameters	4479/0/170	4463/0/167	5259/0/196
Collection range			
<i>h</i>	−11 to 12	−33 to 35	−13 to 13
<i>k</i>	−24 to 24	−12 to 12	−13 to 13
<i>l</i>	−15 to 14	−20 to 17	−14 to 14
GOF on F ²	1.073	1.060	1.047
Final R indexes [I ≥ 2σ (I)]	R ₁ = 0.0429, wR ₂ = 0.1038	R ₁ = 0.0381, wR ₂ = 0.0948	R ₁ = 0.0539, wR ₂ = 0.1317
Final R indexes (all data)	R ₁ = 0.0584, wR ₂ = 0.1132	R ₁ = 0.0498, wR ₂ = 0.1023	R ₁ = 0.0769, wR ₂ = 0.1516
Largest diff. Peak/hole/eÅ ⁻³	0.37/−0.22	0.39/−0.31	0.40/−0.35

3.7. Computational Details

A density functional theory (DFT) molecular orbital calculation (WebMo Pro [20]) with the GAUSSIAN-03 program package [21] employing the B3LYP (Becke three parameter Lee-Yang-Parr exchange correlation functional), which combines the hybrid exchange functional of Becke [22,23] with the gradient correlation functional of Lee, Yang and Parr [21] and the 6–31 G(d) basis set [24] was performed on each of the six compounds. No solvent corrections were made with these calculations. Starting geometries were taken from X-ray refinement data. The optimized results in the free molecule state are, therefore, compared to those in the crystalline state. Discrepancies between the experimental and calculated band centers and band intensities exist. However, this does not prohibit us from making informed decisions on the observations since it is generally known that DFT often underestimates HOMO-LUMO gaps, thereby having a tendency to give excitations far too low in energy. All calculations were performed on a workstation PC using default convergence criteria.

3.8. Density Functional Theory (DFT) Calculations

A comparison of selected bond angles and bond distances in crystals (1), (2) and (3) to that from the geometry optimized DFT calculations at the B3LYP 6–31 G(d) level is given in Tables 1, 3 and 5. The differences between the two values are within normal ranges and generally consistent with bond lengths and angles for similar types of compounds such as in compounds (4), (5) and (6).

In addition, a comparison of the angles between mean planes of the indole and phenylsulfonyl rings in the crystal and with the DFT geometry optimized calculation in concert with strong and weak

intermolecular hydrogen bond interactions has been included in a discussion of the structural aspects for each molecule. From a DFT molecular orbital calculation for each compound, surface plots for the two highest occupied molecular orbital (HOMO and HOMO–1) and three lowest unoccupied molecular orbitals (LUMO, LUMO+1, LUMO+2) are displayed to provide visual evidence of the molecular orbitals involved in the spectroscopic electronic energy transitions examined. Based on correlation of the energies of these HOMO-LUMO frontier surfaces to the UV-VIS absorption spectra, electronic excitation transition predications are suggested.

3.9. Electronic Absorption Spectra

Electronic absorption spectra of all compounds were obtained using a Cary-300 UV-Vis spectrophotometer. All samples were dissolved in acetonitrile and spectra were recorded at room temperature. Stock solutions of $\sim 1 \times 10^{-3}$ M solution were prepared and dilutions were prepared ranging down to $\sim 2 \times 10^{-5}$. All Spectra were scanned from 800 to 190 nm. Deconvolution of the spectra to obtain the λ_{\max} was carried out by the IGOR program [25].

4. Summary and Conclusions

The crystal and molecular structures of three new thiosemicarbazones have been determined, along with the frontier molecular orbitals of each compound displayed through density function theory (DFT-B3LYP 6-31G(d)) geometry optimization and molecular orbital calculations. Structural differences between these three compounds and three closely related previously published compounds have been elucidated. Correlations between the calculated molecular orbital energies (eV) for the surfaces of the frontier molecular orbitals to the electronic excitation transitions from the absorption spectrum of each of the six compounds have been determined. In each compound, the DFT molecular orbital calculation, supported by a geometry optimization calculation, confirmed that the excitation energies of the surfaces of the frontier molecular orbitals from the HOMO–1 and HOMO to LUMO, LUMO+1, LUMO+2, and LUMO+3 electronic excitations in all six compounds closely match the λ_{\max} values of the absorption spectra in overlapping contributions from two, three or four of these excitations within each band envelope. In the crystal structures of the three new compounds, as well as with the three previously published closely related structures, it has been determined that the presence of a methyl or ethyl substituted terminal amine group on the 4-methoxy, 5-ethoxy or 6-methoxy core structures in concert with hydrogen bonds and/or a variety of weak intermolecular interactions play significant roles in the crystal packing of each molecule. This is supported by changes in the mean planes between the hydrazinecarbothioamide group and phenyl rings within each comparative set of structures when the comparison is made between their crystal structures and density functional theory (DFT) geometry optimization calculations.

Supplementary Materials: ^1H , ^{13}C NMR, and UV-vis spectra for all compounds 1–6 are available online at <http://www.mdpi.com/2073-4352/6/2/17/s1>.

Acknowledgments: Jerry P. Jasinski acknowledges the NSF-MRI program (grant No. CHE-1039027) for funds to purchase the X-ray diffractometer. Brian J. Anderson acknowledges the NSF-MRI program (grant No. CHE-1337206) for funds to purchase the 400 MHz NMR spectrometer. The authors also acknowledge Keene State College and the Department of Chemistry for funding and supplies.

Author Contributions: Michael B. Freedman, Sean P. Millikan, Kelly A. O'Rourke, designed the experiments and synthesized the compounds; Brian J. Anderson contributed reagents/materials/analysis tools for the project, interpreted the NMR data and assisted with writing the paper; Victoria A. Smolenski solved and refined the X-ray structures; Jerry P. Jasinski collected the X-ray data, interpreted the crystallographic results, performed the DFT calculations and assisted with writing the paper.

Conflicts of Interest: The authors declare no conflict of interest.

Appendix

CCDC 1445492 (1), 1445493 (2), 1445494 (3) contains supplementary crystallographic data for this paper. These data can be obtained free of charge from The Cambridge Crystallographic Data Centre via www.ccdc.cam.ac.uk/data_request/cif, or by emailing data_request@ccdc.cam.ac.uk, or by contacting The Cambridge Crystallographic Data Centre, 12, Union Road, Cambridge CB2 1EZ, UK; fax: +44-1223-336033. E-Mail: deposit@ccdc.cam.ac.uk or at <http://www.ccdc.cam.ac.uk>.

References

1. Lobana, T.S.; Sharma, R.; Bawa, G.; Khanna, S. Bonding and structure trends of thiosemicarbazone derivatives of metals-an overview. *Coord. Chem. Rev.* **2009**, *253*, 977–1055. [[CrossRef](#)]
2. Ali, M.A.; Livingstone, S.E. Metal complexes of sulfur-nitrogen chelating agents. *Coord. Chem. Rev.* **1974**, *13*, 101–132.
3. Campbell, M.J.M. Transition metal complexes of thiosemicarbazide and thiosemicarbazones. *Coord. Chem. Rev.* **1975**, *15*, 279–319. [[CrossRef](#)]
4. Padhye, S.; Kauffman, G.B. Transition metal complexes of semicarbazones and thiosemicarbazones. *Coord. Chem. Rev.* **1985**, *63*, 127–160. [[CrossRef](#)]
5. Chellan, P.; Nasser, S.; Vivas, L.; Chibale, K.; Smith, G.S. Cyclopalladated complexes containing tridentate thiosemicarbazone ligands of biological significance: Synthesis, structure and antimalarial activity. *J. Organomet. Chem.* **2010**, *695*, 2225–2232. [[CrossRef](#)]
6. Halder, S.; Peng, S.-M.; Lee, G.-H.; Chatterjee, T.; Mukherjee, A.; Dutta, S.; Sanyal, U.; Bhattacharya, S. Synthesis, structure, spectroscopic properties and cytotoxic effect of some thiosemicarbazone complexes of palladium. *New J. Chem.* **2008**, *32*, 105–114. [[CrossRef](#)]
7. Devi, W.B.; Singh, R.K.B.; Jasinski, J.P.; Golen, J.A. A new two dimensional copper(II) coordination complex with sulphonamide: Synthesis, crystal structure and DNA binding study. *Inorg. Chem. Commun.* **2012**, *21*, 163–167. [[CrossRef](#)]
8. Dilworth, J.R.; Hueting, R. Metal complexes of thiosemicarbazones for imagine and therapy. *Inorg. Chim. Acta* **2012**, *389*, 3–15. [[CrossRef](#)]
9. Xie, G.; Chellan, P.; Mao, J.; Chibale, K.; Smith, G.S. Thiosemicarbazone salicylaldiminato-palladium(II)-catalyzed mizoroki-heck reactions. *Adv. Syn. Catal.* **2010**, *352*, 1641–1647. [[CrossRef](#)]
10. Pelagatti, P.; Venturini, A.; Leporati, A.; Carcelli, M.; Costa, M.; Bacchi, A.; Pelizzi, G.; Pelizzi, C. Chemoselective homogeneous hydrogenation of phenylacetylene using thiosemicarbazone and thiobenzoylhydrazone palladium(II) complexes as catalysts. *J. Chem. Soc. Dalton Trans.* **1998**, *16*, 2715–2722. [[CrossRef](#)]
11. Prabhu, R.N.; Ramesh, R. Synthesis and structural characterization of palladium(II) thiosemicarbazone complex: Application to the buchwald-hartwig amination reaction. *Tetrahedron Lett.* **2013**, *54*, 1120–1124. [[CrossRef](#)]
12. Anderson, B.J.; Freedman, M.B.; Millikan, S.P.; Jasinski, J.P. 2-[1-(2-Hydroxy-4-methoxyphenyl)ethylidene]-N-methylhydrazinecarbothioamide. *Acta Crystallogr. Sect. E* **2013**, *69*, o1315. [[CrossRef](#)] [[PubMed](#)]
13. Anderson, B.J.; Keeler, A.M.; O'Rourke, K.A.; Krauss, S.T.; Jasinski, J.P. 2-[1-(2-Hydroxy-6-methoxyphenyl)ethylidene]-N-methylhydrazinecarbothioamide acetonitrile monosolvate. *Acta Crystallogr. Sect. E* **2013**, *69*, o11. [[CrossRef](#)] [[PubMed](#)]
14. Anderson, B.J.; Kennedy, C.J.; Jasinski, J.P. N-Ethyl-2-[1-(2-hydroxy-6-methoxyphenyl) ethylidene] hydrazinecarbothioamide. *Acta Crystallogr. Sect. E* **2012**, *68*, o2982. [[CrossRef](#)] [[PubMed](#)]
15. Anderson, B.; Hall, J.; Jasinski, J. N-ethyl-2-[1-(2-hydroxy-4-methylphenyl) ethylidene] hydrazinecarbothioamide. *Acta Crystallogr. Sect. E* **2014**, *70*, o735. [[CrossRef](#)] [[PubMed](#)]
16. Anderson, B.; Shalit, Z.; Jasinski, J. N-ethyl-2-[1-(2-hydroxynaphthalen-1-yl) ethylidene] hydrazinecarbothioamide. *Acta Crystallogr. Sect. E* **2014**, *70*, o732. [[CrossRef](#)] [[PubMed](#)]
17. Allen, F.H.; Kennard, O.; Watson, D.G.; Brammer, L.; Orpen, A.G.; Taylor, R. Tables of bond lengths determined by X-ray and neutron diffraction. Part I. Bond lengths in organic compounds. *J. Chem. Soc. Perkin Trans.* **1987**, *2*, S1–S19. [[CrossRef](#)]

18. Oxford Diffraction Ltd. *CrysAlis PRO and CrysAlis RED*; Version 1.171.33.34d; Oxford Diffraction Ltd: Abingdon, UK, 2010.
19. Sheldrick, G.M. Crystal structure refinement with SHELXL. *Acta Crystallogr. Sect. C Struct. Chem.* **2015**, *71*, 3–8. [[CrossRef](#)] [[PubMed](#)]
20. WebMO LLC. *WebMO Pro*; Version 8.0.01e; WebMO LLC: Holland, The Netherlands, 2007.
21. Gaussian Inc. *Gaussian 03*; Version C.02; Gaussian Inc.: Wallingford, CT, USA, 2004.
22. Becke, A.D. Density-functional exchange-energy approximation with correct asymptotic-behavior. *Phys. Rev. A* **1988**, *38*, 3098–3100. [[CrossRef](#)] [[PubMed](#)]
23. Lee, C.; Yang, W.; Parr, R.G. Development of the colle-salvetti correlation-energy formula into a functional of the electron density. *Phys. Rev. B Condens. Matter* **1988**, *37*, 785–789. [[CrossRef](#)] [[PubMed](#)]
24. Hehre, W.J.; Random, L.; Schleyer, P.R.; Pople, J.A. Ab initio molecular orbital theory. *Acc. Chem. Res.* **1976**, *9*, 399–406. [[CrossRef](#)]
25. WaveMetrics. *IGOR Pro (1988–2009)*; WaveMetrics: Lake Oswego, OR, USA, 2009.



© 2016 by the authors; licensee MDPI, Basel, Switzerland. This article is an open access article distributed under the terms and conditions of the Creative Commons by Attribution (CC-BY) license (<http://creativecommons.org/licenses/by/4.0/>).